JOURNAL OF MATERIALS SCIENCE 27 (1992) 2770–2780

Some new aspects of the theory of oxidation and degassing of aluminium-based alloy powders

L. KOWALSKI, B. M. KOREVAAR, J. DUSZCZYK
Laboratory for Materials Science, Delft University of Technology, Rotterdamseweg 137, 2628 AL Delft, The Netherlands

A study has been performed of the oxidation and degassing processes of aluminium-based alloy powders. Oxidation and hydration of gas-atomized metal powders take place during in-flight solidification and cooling to room temperature, during collection and keeping in the powder collection box and during transport and storage before consolidation. Under the atomizing conditions, oxidation cannot be prevented. In contact with humid gases (air) the oxide layer on the powder surface takes up water vapour which is physically or chemically bound. A literature study shows that the oxide layer on atomized aluminium powder is amorphous and has a thickness of 2–10 nm depending on the atomizing conditions. The amount of water in the powder is sufficient to form a completely closed hydroxide layer on the outer surface of the powder. The thickness growth of the oxide layer is governed by cation diffusion. Degassing experiments were carried out by heating canned powders in vacuum. The partial pressures of evolved water vapour and hydrogen were registered as a function of temperature at a constant heating rate. Two different alloy powders were used: the first air atomized and containing 1% magnesium (Al–20Si–3Cu–1Mg–5Fe), and the second (Al–9Fe–2Mo–1Zr) magnesium-free powder, atomized by nitrogen. Much work has been done on degassing, but most of it is directed towards industrial applications. The quantitative theoretical description of the degassing phenomenon is still lacking. A new approach aiming at narrowing this gap is presented by employing Wagner's theory of high temperature oxidation of metals. The diffusion coefficient of aluminium cations through the amorphous aluminium oxide layer has been determined in the degassing temperature range by using the experimental data of Hayden *et al.* The diffusion coefficient of aluminium cations through the Al_2O_3 layer has also been evaluated from the degassing experiments. The values obtained directly from the degassing experiments are in reasonable agreement with those derived from the oxidation results. It has been concluded that extrapolation of the results obtained from diffusion experiments at high temperatures in aluminium oxides towards the temperature range of degassing cannot explain the formation of hydrogen during this process, even if the surface diffusion coefficient (much higher than lattice diffusion coefficient) is taken into account.

1. Introduction

Recent studies on gas entrapment and evolution in rapidly solidified aluminium alloy powders have highlighted the role played by the oxide film during degassing [1, 2]. Hence understanding of the phenomena of the oxide layer formation and permeability at the particle surface becomes very important. In the aluminium–oxygen system the partial pressure of oxygen in equilibrium with Al_2O_3 is very small and far below the range attainable in protective gases or in vacuum systems (oxides of aluminium such as Al_2O_3 require an oxygen partial pressure of only 10^{-145} atm at 100 °C and 10^{-39} atm at 900 °C. Therefore, even at very low residual oxygen pressures, oxidation will always take place and the powder particles will be completely covered with an oxide layer. The thickness of this layer will be determined by the available amount of oxygen and by the kinetics of the oxidation process. Important variables are the atomization conditions (air atomization or inert gas atomization), time of flight and temperature history of the particles during atomization, conditions in the powder collection box after atomization and conditions of storage and transport of the powder before degassing and consolidation [3].

The oxidation of aluminium has been proved to be a very complicated process, which is, as yet, not fully understood although much research has been carried out. Hayden *et al.* [4] investigated the initial stages of the oxidation of aluminium at temperatures between 20 and 550 °C and oxygen pressures of 10^{-9}–10^{-2} torr (1 torr = 133.322 Pa). Two oxidation stages were

0022–2461

identified. A fast initial stage was found to correspond to chemisorption and incorporation of oxygen in the metal surface and the formation of a thin amorphous oxide layer via nucleation and growth with a thickness of about 0.3 nm. The formation rate depends on both temperature and oxygen pressure. At room temperature this stage does not go to completion within reasonable measuring times. At elevated temperatures this stage ends after some minutes. The fast formation stage of a closed amorphous oxide layer is followed by a slow thickening stage. At 230–330 °C a logarithmic thickening was found. A layer thickness of 1.5–3.0 nm was reached. At temperatures between 330 and 530 °C the oxidation kinetics were parabolic. Thicknesses of 1.5–4.5 nm were obtained in ~ 5000 s. An activation energy of 113 kJ mol^{-1} (± 5 kJ mol^{-1}) for the thickening rate was determined. The mechanism was ascribed to cation diffusion through the amorphous oxide.

At temperatures above 450 °C and longer oxidation times, crystalline Al_2O_3 is formed by a nucleation and growth process at the aluminium metal surface under the amorphous oxide layer.

2. Oxidation and hydration of atomized powders

2.1. Oxidation

Carney *et al.* [3] investigated the oxide formation of gas-atomized powder. The oxidation process was divided in three stages: (1) in-flight solidification, (2) powder in the collection box and (3) exposure of powder to air.

2.1.1. In-flight solidification

The atomized droplets with a diameter less than 200 μm (median particle size about 20 μm) are rapidly cooled by the atomizing gas. The cooling time was estimated by Estrada *et al.* [1] to be 10^{-5}–10^{-3} s (for particle diameters of 5–100 μm and a gas velocity of 100 m s^{-1}).

Extrapolation of the results of the parabolic thickness growth of the oxide in high-temperature oxidation experiments on aluminium alloys to these very short times gives thickness values far below 0.1 nm. So, although some oxidation must be expected during cooling of the droplets on thermodynamic grounds, only the first fast stage of formation of an amorphous layer can actually take place. This is especially true for atomization by argon or nitrogen gas in which the partial pressure of oxygen is only about 10^{-4}–10^{-5} atm.

At temperatures below ~ 350 °C the thermodynamic conditions for the reaction of aluminium oxide with water vapour become favourable [1, 6, 7]

$$Al_2O_3 + xH_2O \rightarrow Al_2O_3(H_2O)_x \qquad (1)$$

Therefore, this reaction may be expected to take place during atomization in a (humid) air stream. Atomization by inert gas, with its very low water vapour pressure is unlikely to cause this reaction.

2.1.2. Powder in the collection box

In the collection box the powder is at room temperature or at slightly elevated temperature. In a gas-atomization installation the gas atmosphere will be inert and free of water vapour. As the partial pressure of oxygen in the atmosphere will still be above the equilibrium value the oxide formation will proceed at a low rate. After air atomization the conditions for further oxidation are more favourable, while water vapour present in the collection box can also be adsorbed. The mechanism of oxide formation at room temperature on a clean metal surface can be described by Cabrera and Mott's theory [5] for the growth of very thin oxide films. To form an oxide film, metal ions must be removed from the crystal lattice and combined with oxygen ions adsorbed at the metal surface in order to create a new oxide lattice. The transport from the metal lattice is hindered by a strong potential barrier at the metal surface and promoted by an intense electric field which is established between the adsorbed oxygen ions and the underlying metal, causing removal of individual metal cations from their metallic region to interstitial positions in the oxide film. As the thickness of the oxide increases, however, the electric field strength diminishes very sharply. At a certain limiting thickness, the field strength is insufficient to overcome the potential barrier for removal of the metal ions. This limiting thickness is taken to be about 2 nm for aluminium at room temperature. When this thickness is reached the oxidation effectively stops.

The theory described is only applicable while the powder temperature is below about 260 °C. Above this temperature the thermal energy of the aluminium ions is sufficient to overcome the potential barrier for leaving the metal lattice and entering the oxide layer. Hence, above this temperature the oxide film growth will be controlled by the transport of either aluminium ions or oxygen ions through the oxide layer. As mentioned before, the diffusion of aluminium ions may be rate determining for the growth of the initially formed amorphous oxide layers.

2.1.3. Exposure of the powder to air

When the powder is exposed to humid air during transport or storage before consolidation, the oxidation will proceed until the limit set by Cabrera and Mott's theory [5] is reached (assuming that this limit was not reached during atomization). Also water vapour will be bound at the surface of the powder, either as $Al_2O_3 \cdot (H_2O)_x$ or as physically adsorbed water.

2.1.4. Experimental evidence of the oxidation

As an investigation of the oxide layer on the powder particles can only be carried out after completion of the atomization process it is very difficult to separate the three stages described above.

Carney *et al.* [3] investigated high-purity argon gas-atomized powders of different aluminium alloys. Special precautions were taken to prevent contamination

by air during transport from the powder collection box to the electron spectrometer (ESCA) in which the oxide thickness measurements were carried out. The layer thicknesses found varied from 0.7–2 nm, which is below Cabrera and Mott's limit ([5], previous section) for natural oxidation in air (~2 nm). In industrially produced aluminium alloy powders, thicker oxide layers are found. Zhou *et al.* [8] found, for an Al–Fe–Mo–Zr powder produced by nitrogen atomization, an average oxide layer thickness of about 5 nm, which is in agreement with (corrected) earlier results of Estrada *et al.* [1] who, for Al–Si–Cu–Mg powders, found values of the oxide layer thickness of air- and argon-atomized powders of ~7 and 3 nm, respectively. From the oxygen content of Osprey preforms of the same material, an oxide layer thickness on the sprayed droplets of about 1 nm was estimated.

All these thickness values are in the range of the amorphous oxide layer thickness found in slow oxidation experiments [9].

2.2. Hydrogen content of atomized powder

From Estrada *et al.* [1] and Zhou *et al.* [8], the total hydrogen contents of atomized aluminium alloy powders were determined. Estrada *et al.* found 24.5 p.p.m. H in air-atomized Al–Si–Cu–Mg powder, while Zhou *et al.* give the value of 19.8 p.p.m. H in a nitrogen gas-atomized Al–Fe–Mo–Zr powder. These values are far higher than the maximum solubilities of hydrogen in solid and in molten aluminium (0.035 and 0.7 p.p.m., respectively). This leads to the conclusion that practically all hydrogen in the powder is bound in the oxide layer as hydroxides or as adsorbed water vapour. A comparison with the total amount of oxygen (about 0.2 wt %), the thickness of the oxide layer (5–7 nm) and the surface area of the powder (0.3–0.2 $m^2 g^{-1}$) given in References 8 and 1 leads to the conclusion that the amount of hydrogen is just sufficient to saturate the outer layer of the oxide with water.

3. Degassing of aluminium alloy powders

3.1. Degassing procedure

The first processing step applied in this research, for degassing measurements is cold precompaction of the loose powdered alloy into cans as indicated in Fig. 1. The precompaction was carried out on a uniaxial hydraulic press with a rigid die. A compaction pressure of 160 MPa was used in order to provide a material with about 65% of the theoretical density, leaving a proper level of interconnected porosity to allow subsequent degassing to occur efficiently.

Each can contained about 300 g aluminium powder after compaction. A cover plate with an evacuation tube was welded to the end of the can and the evacuation tube was connected to a vacuum source. Fig. 1 shows the arrangement used for degassing a canned powdered alloy. A metallic can (1) is shown containing the PM compact (2). Metallic pads (3) are double welded at the bottom and at the top of the can. The conduit (4) with a filter (5) is welded to the pad of the can and is connected with a vacuum source (turbomolecular pump). Valves (6, 7) are provided so that the canned PM compact can be alternately subjected to degassing treatment under high vacuum, and then to flushing with a depurative gas. The can is placed in a resistance furnace (8). The degassing apparatus contains a set of thermocouples for temperature control and a digital pressure gauge (9) to control the flushing pressure. The cans, pads, and evacuation tubes were made of 6063 (Al–0.4Si–0.7 Mg) aluminium alloy.

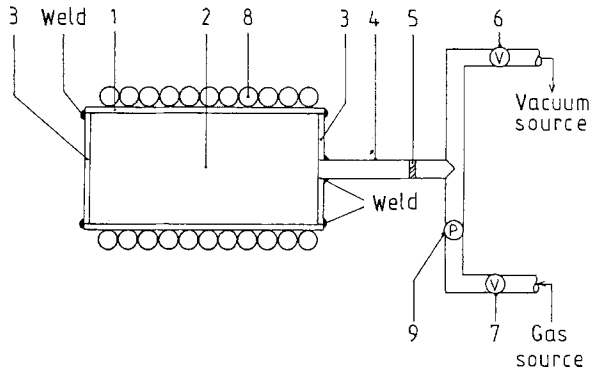

Figure 1 Arrangement used for degassing a canned powdered metal: 1, metallic can; 2, PM compact; 3, metallic pads; 4, evacuation conduit; 5, filter; 6, vacuum valve; 7, gas valve; 8, resistance furnace; 9, digital pressure gauge.

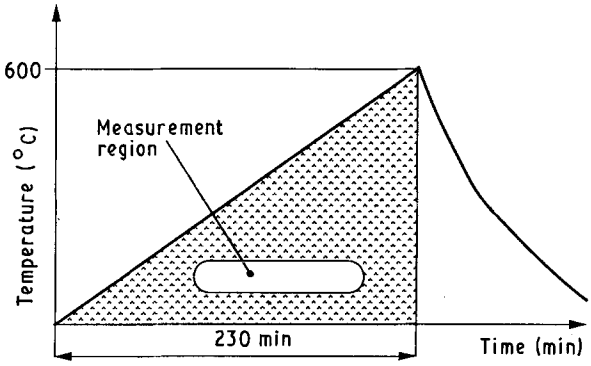

Figure 2 Continuous degassing profile.

The continuous degassing procedure, as depicted in Fig. 2, was adopted. The cans were heated uniformly at a heating rate of about 2.5 °C min^{-1} under high-vacuum conditions up to a temperature exceeding the peak in hydrogen evolution. The water and hydrogen spectra were recorded using a computerized EQ80F Edwards analyser with quadrupole mass spectrometer. The samples, still kept under high-vacuum conditions, were then cooled to room temperature. They were then opened for 24 h to normal atmospheric conditions. Subsequently, the samples were again degassed with analogous parameters as during the first degassing, while recording the evolution of water and hydrogen.

3.2. Material

Two different powders were used during the course of this research. The first, Al–20Si–3Cu–1Mg–5Fe (ASCM-5Fe), was atomized in air, and the second one,

Al–9Fe–2Mo–1Zr, was atomized in a protective nitrogen atmosphere. An extended description of these powders was given in previous papers [8, 10].

3.3. Results

It is noteworthy that the liberation curves of moisture and hydrogen differ substantially for the air-atomized and nitrogen-atomized powders (Figs 3 and 4, respectively). One can see four well-distinguished peaks on the hydrogen liberation curve of the air-atomized powder located at the temperatures 175, 290, 335 and 420 °C. The first three peaks are well correlated with water liberation crests.

There is only one clear maximum for water and hydrogen evolution in the nitrogen-atomized powder. Moreover, the maximum of the hydrogen liberation curve is shifted towards higher temperatures.

The results obtained during the redegassing procedure of the ASCM-5Fe air-atomized powder revealed water and hydrogen evolution runs different from those obtained during the first degassing of this powder (Fig. 5). There is only one peak of water and hydrogen evolution. The redegassing liberation curves for the nitrogen atomized powder had a shape similar to those obtained during the first continuous degassing of this powder.

In order to check whether the hydrogen evolution from aluminium powders is controlled by diffusion, an additional set of experiments was performed on the Strohlein H-mat 251 apparatus [1] with rapidly solidified Al–9Fe–2Mo–1Zr powder. Two different temperatures (300 and 550 °C) were used and different

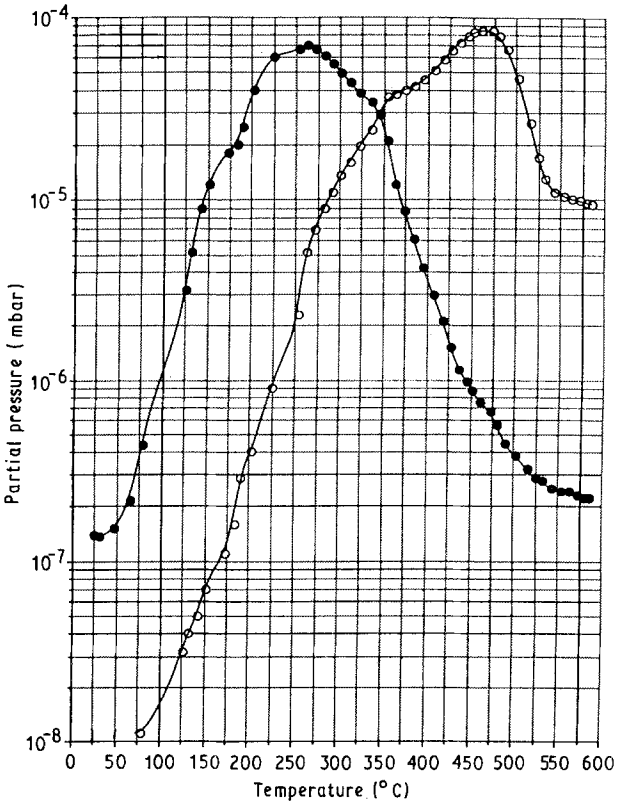

Figure 3 Experimental results from continuous degassing of the Al–9Fe–2Mo–1Zr nitrogen-atomized powder. (○) H_2, (●) H_2O.

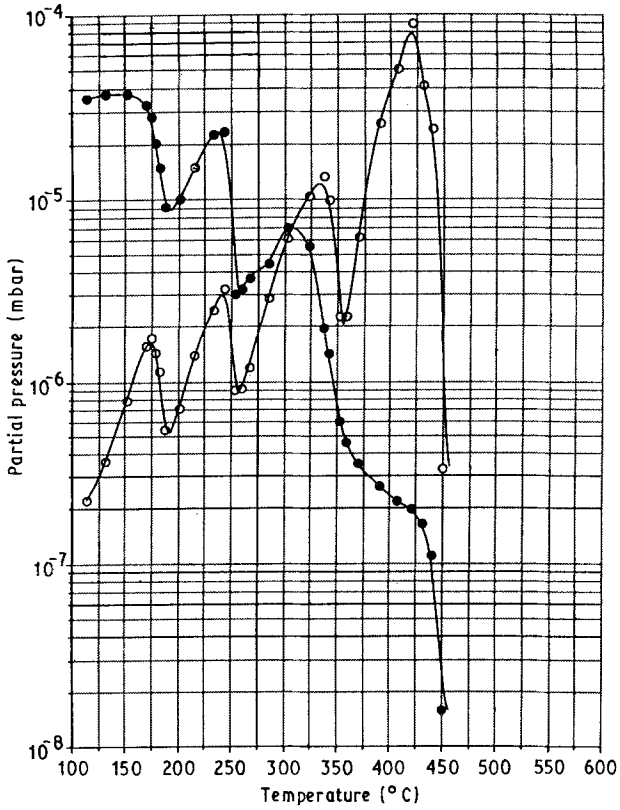

Figure 4 Experimental results from continuous degassing of the ASCM–5Fe air-atomized powder. (○) H_2, (●) H_2O.

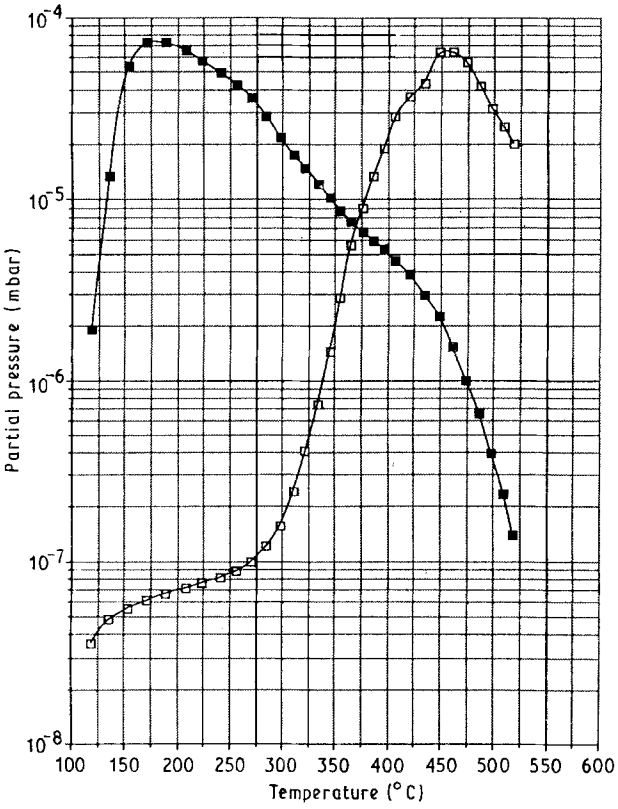

Figure 5 Experimental results from redegassing of the ASCM–5Fe air-atomized powder. (□) H_2, (■) H_2O.

measurement times were adopted (2, 5, 10 and 20 min).

It is apparent that at 550 °C the chemical reaction (oxidation) which results in hydrogen evolution must be very quick – after 2 min more than 40% of the total

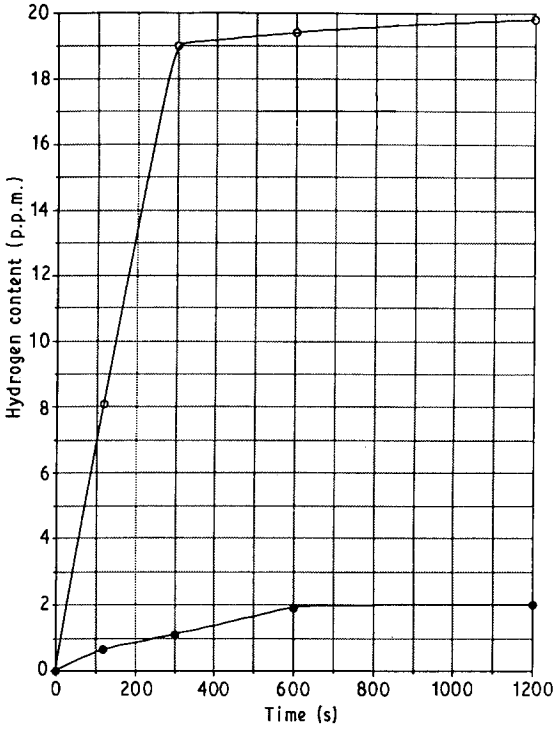

Figure 6 Amount of hydrogen evolved from the sample as a function of time and temperature (Al–9Fe–2Mo–1Zr powder). (○) $T = 550\,°C$, (●) $T = 300\,°C$.

amount of hydrogen is released and after 5 min the evolution of hydrogen seems to be almost completed (see Fig. 6).

4. Discussion

4.1. Chemical reactions during the degassing process

The degassing was carried out in a high vacuum in which the measured pressure of oxygen was about 10^{-12} bar. This is far above the equilibrium pressure for the oxidation reaction of aluminium

$$2Al + 3/2O_2 \rightarrow Al_2O_3 \qquad (2)$$

Thus the oxidation will proceed during the degassing process at a rate determined by the diffusion of aluminium ions through the amorphous oxide layer formed during the production and storage of the powder. At temperatures below 260 °C this rate will be extremely low (see Section 2).

The evolution of water vapour during the degassing is caused by the desorption of physically bound water, in the initial stages of the process, and, later, by the decomposition of aluminium hydroxides. At low temperatures the water molecules are stable; thermodynamic calculations revealed that there is no dissociation of water under degassing conditions, hence there is no contribution to oxygen nor hydrogen evolution originating from this reaction.

The hydrogen evolution during degassing can be ascribed to two different sources.

(i) The liberation of hydrogen dissolved in the powder.

As was argued in Section 2, this is a very small amount, but it may play a part during the initial stages of the degassing.

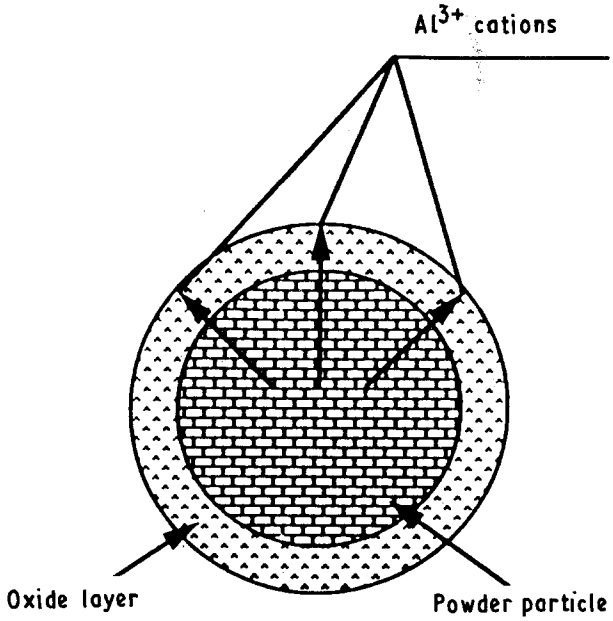

Figure 7 Mechanism of oxidation–migration of aluminium cations from within the bulk of a powder particle.

(ii) The reaction of water vapour with aluminium atoms

$$2Al + 3H_2O \rightarrow Al_2O_3 + 3H_2 \qquad (3)$$

This reaction must take place at the outer surface of the oxide layer. Its rate is determined by the rate of diffusion of aluminium cations through the oxide layer [1] (see Fig. 7). Reaction 3 must compete with Reaction 2 for the available aluminium cations at the oxide surface.

4.2. Diffusion in the oxide layer during degassing

The diffusion through oxide layers has been described by Wagner [11], based on the hypothesis that diffusion in oxides may generally be regarded as migration processes of ions, whereas migration of electrons and electrically neutral atoms or molecules may be neglected.

Assuming that the various particles migrate independently of each other, the average drift velocity, u_i ($cm\,s^{-1}$), of ions of type i in the direction perpendicular to the oxide layer may be described by the expression

$$u_i = -B_i\{(1/N_A)(d\mu/dx) + z_i e(d\Phi/dx)\} \qquad (4)$$

where B_i is the mobility of particles of type i calculated from electrical conductivity data, N_A is the Avogadro number, e is electronic charge, Φ is local electrical potential, μ is chemical potential, z is the electrical valence of a particle of type i, k is Boltzmann's constant and T is the temperature.

For oxide layers thicker than the limiting value in Cabrera and Mott's theory (Section 2), the second term in Equation 4 can be neglected and u_i becomes

$$u_i = (-B_i/N_A)(d\mu/dx)$$
$$= (-B_i/N_A)[d(\mu_0 + RT\ln a_i)/dx] \qquad (5)$$

Equating $B_i = D_i/kT$ (D_i is the diffusion coefficient of ions i) this becomes at constant temperature

$$u_i = -D_i(\mathrm{d}\ln a_i/\mathrm{d}x) \quad (6)$$

Assuming that $\ln a_i$ varies linearly with x, this can be approximated by

$$u_i = D_i[(\ln a_i^m - \ln a_i^g)/h_{ox}] \quad (7)$$

where a_i^m and a_i^g are, respectively, the activities of ions i at the boundaries of the oxide layer with the metal and the gas environment and h_{ox} is the thickness of the oxide layer.

From Equation 7 the number of molecules migrating per unit cross-section per unit time follows

$$n_i = c_i u_i \quad (8)$$

where c_i is the concentration of ions of type i in molecules per unit volume of the oxide. This gives

$$n_i = D_i c_i[(\ln a_i^m - \ln a_i^g)/h_{ox}] \quad (9)$$

For the diffusion of aluminium ions from the metal boundary to the oxide surface, a_{Al}^m at the metal boundary can be taken equal to one, which gives

$$n_{Al} = D_{Al}c_{Al}(-\ln a_{Al}^g/h_{ox}) \quad (10)$$

4.3. Values of the diffusion coefficients

The basic problem with the evaluation of Equations 9 and 10 is the quantitative determination of the diffusion coefficients to use in these equations. Reliable data on the diffusion coefficients in aluminium oxide in the temperature range for degassing of PM aluminium alloys are not available in the literature.

The diffusion coefficient of aluminium in aluminium oxide over the temperature range 1670–1905 °C is given by [12]

$$D = 28\exp(-490\,000/RT) \quad \mathrm{cm^2\,s^{-1}} \quad (11)$$

where T is the absolute temperature and R is the universal gas constant ($\mathrm{J\,mol^{-1}}$). For the diffusion coefficient of oxygen, approximately the same value was found. Extrapolation to the temperature range for degassing leads, however, to extremely low values, which make the growth of oxides by diffusion virtually impossible. Moreover this high value of the activation energy for diffusion strongly deviates from the activation energies determined for the parabolic growth of aluminium oxides, for which very different values are given in the literature, for example: $Q = 113 \pm 5\ \mathrm{kJ\,mol^{-1}}$ [4], $226\ \mathrm{kJ\,mol^{-1}}$ [13], $155.6\ \mathrm{kJ\,mol^{-1}}$ [14], $95.4\ \mathrm{kJ\,mol^{-1}}$ [15], $108.8\ \mathrm{kJ\,mol^{-1}}$ [16]. On the basis of these results it is generally accepted that high diffusivity paths exist in the oxide layers, which enhance the growth rate.

4.4. Surface diffusion

The oxide layer has been built up from amorphous nuclei that grow laterally along the metal surface until they impinge on each other, forming some kind of boundary perpendicular to the metal surface. When a fully closed layer has been formed, further growth takes place in a direction perpendicular to the surface. It may be assumed that this columnar growth of amorphous matter with many column boundaries can be described by a diffusion mechanism which is closely related to the surface diffusion along an amorphous boundary. The surface diffusion coefficients of oxides have been determined by several investigators [17]. In Fig. 10 from [17] an estimated value is given for the surface diffusion coefficient of aluminium as a function of T. From this figure the following formula was derived for the surface diffusion coefficient

$$D_{Al} = 1.486\times10^{-5}\exp(-223\,400/8.314\,T)\ \mathrm{cm^2\,s^{-1}} \quad (12)$$

The surface diffusion coefficients for different temperatures are given in Table I.

TABLE I Activity of aluminium at the oxide surface and the diffusion coefficient of aluminium through the oxide layer calculated from the oxidation results–comparison with the surface diffusion coefficient

Temperature (°C)	Activity, a_{Al}^g	D_{Al} (calc. from [4]) ($\mathrm{cm^2\,s^{-1}}$)	D_{Al}^s (surface diffusion coeff.) ($\mathrm{cm^2\,s^{-1}}$)
22	1.69×10^{-151}	1.13×10^{-32}	4.11×10^{-45}
100	1.42×10^{-120}	2.17×10^{-28}	7.69×10^{-37}
200	7.55×10^{-96}	6.07×10^{-25}	3.17×10^{-30}
300	9.44×10^{-80}	1.10×10^{-22}	6.40×10^{-26}
400	1.93×10^{-68}	4.35×10^{-21}	6.80×10^{-23}
500	4.69×10^{-60}	6.77×10^{-20}	1.19×10^{-20}

4.5. Calculation of diffusion coefficient from oxidation results given by Hayden *et al.* [4]

In the temperature region between 330 and 530 °C at a pressure of 10^{-4} torr, Hayden *et al.* [4] found a parabolic oxidation rate $X^2 = kt$, in which $k = k_0 e^{-Q/RT}$. For Q the value $113\,000\ \mathrm{J\,mol^{-1}}$ ($\pm 5000\ \mathrm{J\,mol^{-1}}$) was given. From Hayden's Fig. 9, a value was derived for k_0: $4\times10^{-10}\ \mathrm{cm^2\,s^{-1}}$

$$X^2 = \{4.1\times10^{-10}\exp(-113\,000/8.314\,T)\}t\ \mathrm{cm^2} \quad (13)$$

where t is the time of oxidation. The thickness of the amorphous oxide was maximally about 2 nm.

According to Wagner's theoretical treatment of parabolic oxidation [11] k is approximately

$$k = [1/(RT)]\int_{\mu_i^g}^{\mu_i^m} D_i\,\mathrm{d}\mu_i \quad (14)$$

in which μ_i^g and μ_i^m are the chemical potentials of species i at the gas–oxide boundary and at the oxide–metal boundary. If D_i is taken to be independent of μ_i then

$$k_i = (D_i/RT)(\mu_i^m - \mu_i^g) \quad (15)$$

or

$$k_i = (D_i/RT)RT(\ln a_i^m - \ln a_i^g) \quad (16)$$

$$k_i = D_i(\ln a_i^m - \ln a_i^g) \quad (17)$$

or

$$D_i = k_i/(\ln a_i^m - \ln a_i^g) \quad (18)$$

in which a_i is the activity of species i. a_{Al}^g can be derived from the reaction equation:

$$4/3\,Al + O_2 \rightarrow 2/3\,Al_2O_3 \quad (19)$$

for which

$$\Delta G = \Delta G_0 + RT\ln K$$

$$= -1113\,500 + 205.5\,T + RT\ln\left\{\frac{(a_{Al_2O_3})^{2/3}}{[p_{O_2}(a_{Al})^{4/3}]}\right\} \quad (20)$$

where K is the equilibrium constant.

Thermodynamic data were taken from Barin and Knacke [18]. The oxygen pressure during the experiments was 1.0×10^{-4} torr or 1.33×10^{-7} atm. If $a_{Al_2O_3}$ is taken to be unity, then

$$a_{Al}^g = [1/(K p_{O_2})]^{3/4} \quad (21)$$

When a_{Al}^m is taken to be unity, D_{Al} can be calculated from Equation 18. The results of this calculation are given in Table I. D_{Al} is given by

$$D_{Al} = 8.2 \times 10^{-12}\exp(-117\,800/8.314\,T)\ cm^2\,s^{-1} \quad (22)$$

4.6. Diffusion coefficient calculated from degassing results

The Al–Fe–Mo–Zr powder fabricated by nitrogen atomization contains about 20 p.p.m. hydrogen [8]. For 300 g powder in the degassing can, this is 6×10^{-3} g hydrogen. 6×10^{-3} g H is equivalent to 54×10^{-3} g H_2O or 0.003 gmol H_2O or $0.003 \times 6.023 \times 10^{23} = 1.81 \times 10^{21}$ molecules. These are removed in the form of H_2O or H_2 by the vacuum pump during degassing, which takes, at a temperature rise from 25 °C to 600 °C at a rate of 2.5 °C min^{-1}, about 13 800 s. The instantaneous pressures of water and hydrogen in the system with a volume of $\sim 1000\ cm^3$ taken from Fig. 4 are given in Table II. The numbers of gas molecules are calculated from the pressures, using the formula

$$n = V_0\{(N_A/\text{mol}\,V_0)[(p\,T_0)/(p_0\,T)]\} \quad (23)$$

where N_A is Avogadro's number, p_0, T_0 are the standard conditions (1 atm, 295 K), V_0 is the volume of the system, mol V_0 is the molar volume at 295 K and 1 atm.

The number of molecules evolved during the whole degassing process can be estimated from

$$\int_0^{t_c} nv\,dt = 1.81 \times 10^{21} \quad (24)$$

where n is the number of gas molecules in the system at time t, v is the pumping velocity. This can be approximated by

$$\sum nv\frac{t}{m} = 1.81 \times 10^{21} \quad (25)$$

where m is the number of steps for the summation. In this equation, n is proportional to the pressure in the system and v will be proportional to the square root of the pressure (gradient) according to Bernoulli's law. Thus

$$C\sum n^{3/2}\frac{t}{m} = 1.81 \times 10^{21} \quad (26)$$

in which the constant C is found to be 1.3×10^{-5}.

The numbers of hydrogen molecules evolving per second from the powder are given in Table III. According to the reaction equation

$$2/3\,Al + H_2O \rightarrow 1/3\,Al_2O_3 + H_2 \quad (27)$$

with

$$\Delta G = \Delta G_0 + RT\ln K \quad (28)$$

every aluminium ion coming to the oxide surfaces frees 1.5 H_2 molecules. The minimum number of aluminium ions arriving at the oxide surface per second at different temperatures is given in Table III. Applying Equation 10

$$n_{Al} = -D_{Al}c_{Al}(\ln a_{Al}^g)S/h_{ox} \quad (29)$$

D_{Al} can be calculated with $c_{Al} = 3.764 \times 10^{22}$, $h_{ox} = 5 \times 10^{-7}$ cm, surface area of the powder $S = 9.27 \times 10^5\ cm^2$.

The aluminium activity, a_{Al}^g, obtained from Equation 27 is given by

$$a_{Al}^g = [p_{H_2}/(p_{H_2O}K)]^{3/2} \quad (30)$$

with [20]

$$\Delta G_0 = -315\,540 + 60\,T\ J\,mol^{-1} \quad (31)$$

The results are given in Table III.

Other values for n_{Al} and D_{Al} can be obtained from Fig. 6 for the temperatures 300 and 550 °C, which are also given in Table III. Using the D_{Al} values for 100, 200, 300* and 550* °C, that are probably the most

TABLE II Partial pressures and numbers of water and hydrogen molecules as a function of degassing temperature

Temperature (°C)	p_{H_2O} (bar)	p_{H_2} (bar)	n_{H_2O} (mol)	n_{H_2} (mol)	$n_{H_2O+H_2}$ (mol)
22	1.4×10^{-10}	2.0×10^{-12}	3.50×10^{12}	5.07×10^{10}	3.55×10^{12}
100	1.1×10^{-9}	1.6×10^{-11}	2.17×10^{13}	3.16×10^{11}	2.20×10^{13}
200	4.0×10^{-8}	4.0×10^{-10}	6.24×10^{14}	6.24×10^{12}	6.30×10^{14}
300	5.0×10^{-8}	1.3×10^{-8}	6.44×10^{14}	1.67×10^{14}	8.11×10^{14}
400	3.2×10^{-9}	5.0×10^{-8}	3.51×10^{13}	5.48×10^{14}	5.38×10^{14}
500	4.0×10^{-10}	4.0×10^{-8}	3.82×10^{12}	3.82×10^{14}	3.86×10^{14}
600	2.0×10^{-10}	9.0×10^{-9}	1.69×10^{12}	7.56×10^{13}	7.77×10^{13}

TABLE III Numbers of water and hydrogen molecules evolving per second from the powder

Temperature (°C)	n_{H_2O} (mol s^{-1})	n_{H_2} (mol s^{-1})	n_{Al} (ion s^{-1})	D_{Al} (cm^2 s^{-1})
22	1.1×10^{15}	1.5×10^{13}	1.00×10^{13}	7.60×10^{-26}
100	6.7×10^{15}	9.8×10^{13}	6.53×10^{13}	6.32×10^{-25}
200	1.9×10^{17}	1.9×10^{15}	6.26×10^{15}	7.70×10^{-23}
300	2.0×10^{17}	5.2×10^{16}	3.43×10^{16}	5.43×10^{-22}
400	1.1×10^{16}	1.7×10^{17}	1.13×10^{17}	2.33×10^{-21}
500	1.2×10^{16}	1.2×10^{17}	8.00×10^{16}	2.05×10^{-21}
600	1.2×10^{15}	3.0×10^{17}	2.00×10^{17}	5.91×10^{-22}
300*	–	3.5×10^{17}	2.30×10^{17}	1.86×10^{-21}
550*	–	6.9×10^{18}	4.00×10^{18}	1.09×10^{-19}

* Derived from Fig. 6.

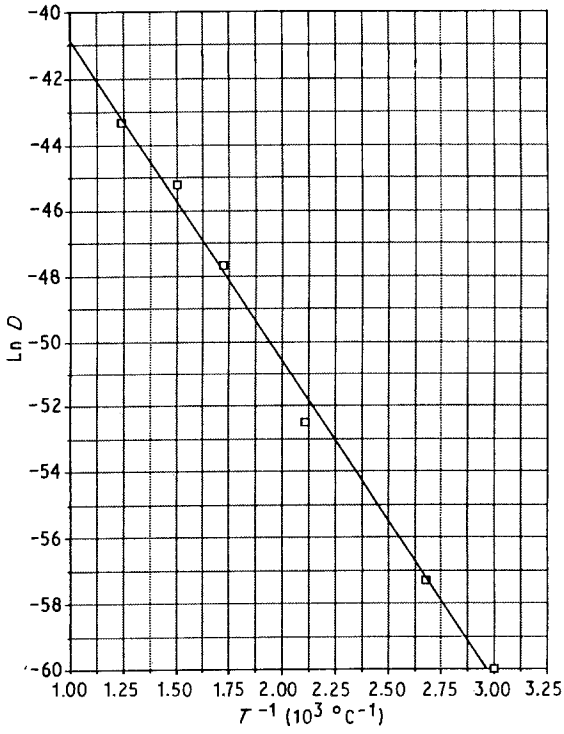

Figure 8 Ln D_{Al} as a function of $10^3/T$. $y = 31.079–9.7570x$, $R^2 = 0.995$.

reliable (Fig. 8), the expression

$$D_{Al} = 2.89 \times 10^{-14} \exp(-80\,620/8.314\,T) \text{ cm}^2 \text{ s}^{-1} \quad (32)$$

was obtained. Recalculating n_{Al} and D_{Al} using Equations 10 and 32 gives the results shown in Table IV. A comparison of the recalculated D_{Al} and n_{Al} with the experimental values in Table III shows rather large deviations at room temperature and at 500 and 600 °C. The first can partly be explained by take-off effects of the experiment (see Fig. 4). Another reason for the high value at room temperature could be the liberation of dissolved hydrogen from the powder. The deviations at high temperatures are caused by the diminishing evolution of water vapour and hydrogen at these temperatures (Fig. 4 and Table II), so that only some of the aluminium ions arriving at the oxide surface are used to form hydrogen.

The values found for D_{Al} are in reasonable agreement with those derived from the experiments of

TABLE IV Recalculated values of D_{Al} and n_{Al}

Temperature (°C)	D_{Al} (cm^2 s^{-1})	n_{Al} (mol s^{-1})
22	1.70×10^{-20}	2.20×10^{9}
100	1.68×10^{-25}	1.66×10^{12}
200	3.85×10^{-23}	3.13×10^{14}
300	1.36×10^{-21}	8.61×10^{15}
400	1.67×10^{-20}	8.12×10^{16}
500	1.07×10^{-19}	4.18×10^{17}
550	2.29×10^{-19}	8.39×10^{17}
600	4.49×10^{-19}	1.52×10^{18}

Hayden *et al.* (Table I) at temperatures above 300 °C. With this comparison it must be taken into account that Hayden's values were derived from oxidizing experiments above 300 °C. Below this temperature region, Hayden *et al.* found another growth mechanism with a lower activation energy [4].

The values for the surface diffusion coefficient, given in Table I, are also of the right order of magnitude at the higher temperatures but too low in the temperature region below 400 °C to explain the hydrogen formation during degassing.

4.7. Degassing experiments

4.7.1. Nitrogen-atomized Al–Fe–Mo–Zr powder

The degassing curves of this material show a regular behaviour. The evolution of water vapour first increases exponentially with increasing temperature. Above 200 °C the evolution slows down and a maximum is reached at about 270 °C. After a small decline up to 350 °C another maximum (of $p_{H_2O} + p_{H_2}$) is attained at 470 °C. Above this maximum the H_2O (H_2) production falls off, but still proceeds at an appreciable rate at 600 °C. Based on the investigations by Litvintsev and Arbuzova [6] these maxima are ascribed to the decomposition of

$$Al_2O_3 \cdot 3H_2O \rightarrow Al_2O_3 \cdot H_2O + 2H_2O \quad (33)$$

in the temperature region 170–350 °C, and of

$$Al_2O_3 \cdot H_2O \rightarrow \gamma Al_2O_3 + H_2O \quad (34)$$

in the temperature region 400–600 °C.

The evolution of water vapour below 170 °C, which shows a secondary peak around 150 °C can be caused by the liberation of physically bound water.

The formation of hydrogen has already begun at room temperature at a rate that is difficult to explain by the diffusion of aluminium ions through the oxide layer. It was suggested earlier that the evolution of dissolved hydrogen could be responsible for the early hydrogen formation. Above about 100 °C the diffusion rate of aluminium ions through the oxide layer is sufficiently large to account for the evolved hydrogen. Below 250 °C, the water vapour production rises at about the same rate as the aluminium diffusion speed, so that the ratio of p_{H_2O}/p_{H_2} stays approximately constant. Above 250 °C the aluminium diffusion increases faster than the water vapour production and an increasing part of the water vapour is transformed into hydrogen.

4.7.2. Air-atomized Al–Si–Cu–Mg–5Fe powder

The results of the initial degassing experiment on the air-atomized ASCM–5Fe powder, given in Fig. 3, differ markedly from those of the degassing experiment on the nitrogen-atomized powder Al–Fe–Mo–Zr given in Fig. 4. A first effect is a general shift of the water evolution curve to lower temperatures of about 100 °C. A second effect is the appearance of a pronounced maxima in the water evolution curve at ~130, 230 and 335°C. Corresponding maxima, although shifted to slightly higher temperatures, are found in the hydrogen evolution which also has a fourth maximum at about 425 °C.

The water vapour and hydrogen pressures integrated over the temperature range of the degassing experiment are lower than for the Al–Fe–Mo–Zr powder although the total hydrogen content of the ASCM–5Fe powder amounts about 24 p.p.m. [10] compared with 20 p.p.m. for the Al–Fe–Mo–Zr powder [8].

The redegassing curves when the ASCM-5Fe powder was cooled to room temperature after the first degassing experiment and then exposed to normal atmospheric conditions for 24 h show only one maximum in the water vapour evolution and also only one maximum in the hydrogen formation (Fig. 5). These curves show a resemblance to the degassing curves of the nitrogen-atomized Al–Fe–Mo–Zr powder, although the maximum of the water evolution curve is positioned at a temperature about 75 °C lower. The total amount of water evolved as determined by the integration of the summated curves over the temperature range of the degassing run is larger than that of the first run and approximately equal to that of the nitrogen-atomized powder in its first degassing run.

Explanations of the different behaviour of the air-atomized powder in the first degassing run can, without further experimental analyses, only be of a very speculative nature. It can be accepted that the oxide layer of the magnesium-containing air-atomized powder has a different structure than that of the magnesium-free nitrogen-atomized powder. The oxide layer has been found to be thicker after air atomizing than after nitrogen atomizing (thickness about 7 and 5 nm, respectively). Auger analysis of the oxide surface composition gave a magnesium content at the oxide surface of about 20%, compared to 1% in the metal [10]. This is caused by the greater stability of MgO in comparison with Al_2O_3 and by the faster diffusion of magnesium through the oxide layer. The four maxima in the $H_2O + H_2$ evolution with increasing temperature can be very tentatively ascribed to:

(i) desorption of adsorbed water molecules (below 175 °C),

(ii) decomposition of $Al_2O_3 \cdot 3H_2O$ to $Al_2O_3 \cdot 2.5H_2O$ (200–250 °C),

(iii) decomposition of $Al_2O_3 \cdot 2.5H_2O$ to $Al_2O_3 \cdot 1H_2O$ (260–350 °C),

(iv) decomposition of $Al_2O_3 \cdot 1H_2O$ (350–450 °C).

The diffusion coefficients of metal ions through the oxide layer were calculated as described in the preceding section. The results are given in Table V and Fig. 9.

A comparison with the diffusion coefficients derived for the Al–Fe–Mo–Zr powder (drawn line in Fig. 9, and Table IV) show a satisfactory agreement for the temperatures of 200 °C and higher. The values at 100 and 150 °C are too large in comparison. A possible explanation could be the evolution of hydrogen dissolved in the metal powder. The larger diffusivity of magnesium in the oxide layer could also affect the results. The maxima and minima in the hydrogen formation are directly related to the maxima and

TABLE V Numbers of hydrogen molecules formed per second in the powder, the corresponding numbers of aluminium ions coming to the oxide surface and the derived diffusion coefficient, D_{Al}

ASCM-5Fe, first run				ASCM-5Fe, second run			
Temperature (°C)	n_{H_2} (molecules s^{-1})	n_{Al} (ion s^{-1})	D_{Al} ($cm^2 s^{-1}$)	Temperature (°C)	n_{H_2} (molecules s^{-1})	n_{Al} (ion s^{-1})	D_{Al} ($cm^2 s^{-1}$)
100	3.91×10^{13}	2.61×10^{13}	6.77×10^{-24}	125	4.44×10^{12}	2.96×10^{12}	8.20×10^{-25}
150	3.28×10^{14}	2.19×10^{14}	6.50×10^{-23}	150	6.19×10^{12}	4.12×10^{12}	1.19×10^{-24}
200	2.50×10^{14}	1.67×10^{14}	5.70×10^{-23}	200	7.90×10^{12}	5.30×10^{12}	1.74×10^{-24}
250	6.76×10^{14}	4.51×10^{14}	1.74×10^{-22}	250	9.32×10^{12}	6.21×10^{12}	2.24×10^{-24}
300	4.71×10^{15}	3.14×10^{14}	1.37×10^{-22}	300	1.12×10^{13}	7.48×10^{12}	3.01×10^{-24}
350	2.26×10^{15}	1.51×10^{15}	7.49×10^{-22}	350	8.02×10^{14}	5.35×10^{14}	2.50×10^{-22}
400	6.38×10^{16}	4.25×10^{15}	2.49×10^{-20}	400	2.58×10^{16}	1.72×10^{16}	9.34×10^{-21}
420	1.73×10^{17}	1.15×10^{17}	7.14×10^{-20}	450	1.19×10^{17}	7.91×10^{16}	4.08×10^{-21}

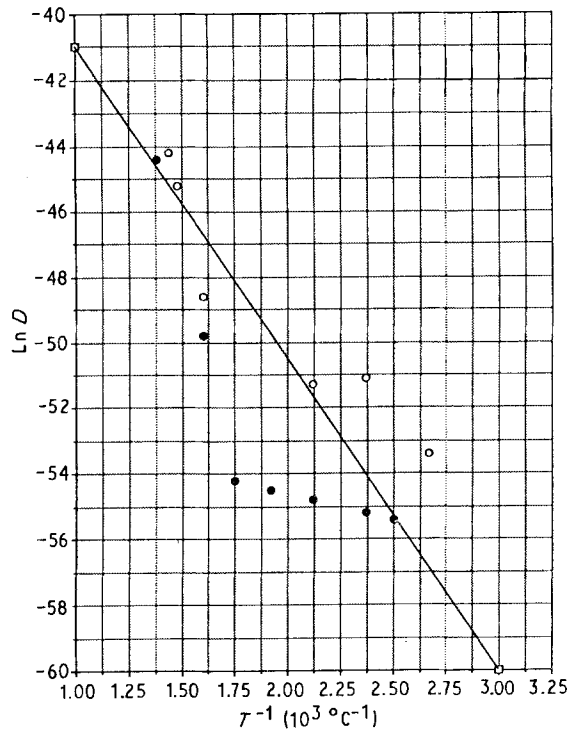

Figure 9 Comparison of the calculated diffusion coefficients for the (□——□) Al–9Fe–2Mo–1Zr and (○, ●) ASCM–5Fe powders. (○) First run, (●) second run.

minima in the water evolution through the equilibrium constant

$$K = p_{H_2}/\{p_{H_2O}(a_{Al})^{2/3}\} \quad (35)$$

from Equation 27. The fast decrease in the water evolution after the maxima cannot be fully compensated by the slower increase of a_{Al} as a consequence of the increasing of the aluminium-ion diffusion with temperature. Thus the hydrogen diffusion must fall off parallel to water evolution, although relatively less because of the increase in a_{Al} with temperature.

During the exposure of the once degassed powder to (moist) air at room temperature, water is again adsorbed at the oxide surface. At this low temperature the water molecules will be preferentially bound in the simpler forms, first as physically adsorbed water, in the more advanced stage as $Al_2O_3 \cdot 1H_2O$ and finally as $Al_2O_3 \cdot 3H_2O$. This is confirmed by the results of the degassing experiment (Fig. 5), where the water evolution shows only one clear maximum at 175 °C in the region earlier ascribed to the desorption of physically bound water. A second maximum of water evolution shown by the maximum of hydrogen formation appears at 450 °C in the region of the decomposition of $Al_2O_3 \cdot 1H_2O$. The shift of the water evolution curve to higher temperatures may be due to the presence of a higher concentration of magnesium at the oxide surface, which was transported to the surface during the first degassing treatment. The formation of hydrogen in the redegassing experiment starts at a much higher temperature than in the first degassing run. The absence of dissolved hydrogen in the powder can be partly responsible for this phenomenon. A second reason might be a slower diffusion of metal ions in the annealed and slowly cooled oxide layer. This is suggested by the low values of the diffusion coefficients at the lower temperatures (see Table V and Fig. 9) derived from the hydrogen formation in the second degassing run. Above 350 °C the diffusion coefficients are the same as in the first degassing run.

5. Conclusions

1. Hydrogen in solution in aluminium alloy powders after atomization can only play a minor part in the hydrogen evolution during degassing.

2. The oxide layer on the powder particles after atomization is amorphous and contains physically adsorbed and chemically bound water in a sufficient amount to form a layer one molecule thick on the surface.

3. The growth of the oxide layers is governed by aluminium ion diffusion through the layers. The diffusion rate through the layers greatly exceeds the diffusion rate in massive crystalline aluminium oxide. From oxidation experiments [4], values for the diffusion coefficients of aluminium through amorphous Al_2O_3 have been derived for the degassing temperature range.

4. Hydrogen formation during degassing is controlled by the diffusion of aluminium ions through the oxide layer to the oxide surface.

5. Values of the diffusion coefficient of aluminium ions through the Al_2O_3 layer have been calculated from the hydrogen formation rates during degassing. These are in reasonable agreement with those derived from the oxidation experiments within the temperature range of parabolic oxide growth rates.

6. The surface diffusion coefficients of aluminium on Al_2O_3 derived from data given by Ikuma and Komatsu [17] were too small in the temperature range below 400 °C to account for the hydrogen formation during degassing.

7. The water vapour and hydrogen evolution curves for nitrogen-atomized Al–9Fe–2Mo–1Zr powder and air-atomized Al–20Si–3Cu–1Mg–5Fe powder, differ markedly. The degassing curves of the Al–Fe–Mo–Zr powder show a regular behaviour, whereas those of the Al–Si–Cu–Mg–Fe powder exhibit well-pronounced maxima which, supposedly, may be attributed to the desorption of water (below 175 °C) and decomposition of hydroxides (200–450 °C).

8. During redegassing after exposure to (moist) air, the behaviour of the air-atomized powder was similar to that of the nitrogen-atomized powder in the first degassing experiment.

References

1. J. L. ESTRADA, J. DUSZCZYK and B. M. KOREVAAR, *J. Mater. Sci.* **26** (1991) 1431.
2. S. D. KIRCHOFF, J. Y. ADKINS, W. M. GRIFFITH and I. A. MARTORELL, in "Rapidly Solidified Powder Aluminium Alloys", ASTM STP 890, edited by M. E. Fine and E. A. Starke (American Society for Testing and Materials, Philadelphia, PA, 1986) p. 354.
3. T. J. CARNEY, P. TSAKIROPOULOS, J. F. WATTS and J. E. CASTLE, *Int. J. Rapid Solid.* **5** (1990) 189.

4. B. E. HAYDEN, W. WYROBISCH, W. OPPERMANN, S. HACHICHA, P. HOFMANN and A. M. BRADSHAW, *Surface Sci.* **109** (1981) 221.
5. N. CABRERA and N. F. MOTT, *Rep. Progr. Phys.* **12** (1948/49) 163.
6. A. L. LITVINTSEV and L. A. ARBUZOVA, *Poroskhovaya Metallurgiya* **49** (1967) 1.
7. L. ACKERMANN, I. GUILLEMIN, R. LALAUZE and C. PIJOLAT, in "High Strength Powder Metallurgy Aluminium Alloys II", edited by G. J. Hildeman and M. J. Koczak (The Metallurgical Society of AIME Warrendale, PA, 1986) p. 175
8. J. ZHOU, J. DUSZCZYK and B. M. KOREVAAR, *J. Mater. Sci.* **26** (1991) 3292.
9. K. SHIMIZU, R. C. FURNEAUX, G. E. THOMPSON, G. C. WOOD, A. GOTOH and K. KOBAYASHI, *Oxid. Metals* **35** (1991) 427.
10. J. L. ESTRADA and J. DUSZCZYK, *J. Mater. Sci.* **25** (1990) 886.
11. C. WAGNER, in "Atom Movements" (American Society for Metals, Cleveland, OH, 1951) p. 153.
12. A. E. PALADINO and W. D. KINGERY, *J. Chem. Phys.* **37** (1962) 957.
13. A. F. BECK, M. A. HEINE, E. J. CANLE and M. J. PRYOR, *Corros. Sci.* **7** (1967) 1.
14. W. W. SCHMELTZER, *J. Electrochem. Soc.* **103** (1956) 209.
15. E. A. GULBRANSEN and W. S. WYSONG, *J. Phys. Colloid Chem.* **57** (1947) 10187.
16. R. K. HART and J. K. MAURIN, *Surface Sci.* **20** (1970) 285.
17. Y. IKUMA and W. KOMATSU, *Mater. Sci. Forum* **29** (1988) 199.
18. J. BARIN and O. KNACKE, in "Thermochemical Properties of Inorganic Substances" (Springer Verlag, Berlin, 1973).

Received 19 September
and accepted 26 September 1991